

# Surface properties of $\text{Co}_2\text{VO}_4$

Percy Ngobeni<sup>1\*</sup>, Phuti Ngoepe<sup>2</sup>, and Khomotso Maenetja<sup>1</sup>

Materials Modelling Centre, University of Limpopo, South Africa

**Abstract.** Increasing oil prices and the challenges posed by global warming have driven us to seek modern approaches to energy storage and consumption, such as the development of smart grid technology. Additionally, as portable electronic devices rapidly evolve, there is a growing demand for more powerful sources and increased energy supply. Innovative energy storage solutions, like zinc-air batteries, offer potential alternatives to metal-ion batteries. We aim to use the  $\text{Co}_2\text{VO}_4$  as a catalyst for Zinc-air batteries by employing the Density Functional Theory (DFT) to study its bulk structure and surface properties. The structural properties, including the lattice parameters and bond lengths, were determined and compared favorably with those from the literature. The electronic properties reveal the metallic behavior of the  $\text{Co}_2\text{VO}_4$  system, with the d orbitals for vanadium and cobalt atoms overlapping at the Fermi level observed. The optimized bulk structure of  $\text{Co}_2\text{VO}_4$  serves to cleave lower Miller index surfaces and assess their stability. We will gain a deeper understanding of the functionality of the  $\text{Co}_2\text{VO}_4$  surfaces.

## 1 Introduction

Because they utilize oxygen from the air for their chemical processes, metal-air batteries are considered efficient for storing energy [1]. Metal-air batteries differ from conventional batteries by incorporating a metal anode for one component and a porous air cathode for the other, rather than using solid materials throughout both parts. Oxygen can be utilized as the battery operates and is restored during the charging process due to this design [2]. Zinc-air batteries (ZABs) are increasingly favored for their ability to store large amounts of energy, their sustainability, and their low cost [3]. They function by employing oxygen reduction reactions (ORR) to produce energy and using oxygen evolution reactions (OER) to accumulate energy. These processes are slow due to their complex steps, which involve transferring multiple electrons, sluggish kinetics of ORR and OER at the cathode limit the lifespan of zinc-air batteries.

Mu et al [4] reported a spinel  $\text{Co}_2\text{VO}_4$  catalyst that combines metallic vanadium atomic chains with low-spin  $\text{Co}^{2+}$  cations at octahedral sites, enhancing oxygen reduction reaction (ORR) activity and electrical conductivity by several orders of magnitude compared with conventional cobalt oxides. When used in a zinc-air battery,  $\text{Co}_2\text{VO}_4$  achieved a record discharge peak power density of  $380 \text{ mW cm}^{-2}$ , surpassing Pt/C-based systems and all previously reported metal, metal oxide, and carbon catalysts. This work demonstrates a viable

---

\* Corresponding author: [khehlapercy0@gmail.com](mailto:khehlapercy0@gmail.com)

strategy for designing highly active, conductive oxide catalysts for ORR and other electrochemical energy conversion reactions.

There is growing interest in spinel-type transition metal oxides as catalysts for two key processes: the ORR and the OER. This occurs because they possess adaptable electronic features, can participate in various chemical reactions, and maintain stability in basic environments [5]. In particular,  $\text{Co}_2\text{VO}_4$ , a cobalt-vanadium mixed oxide with an inverse spinel structure, offers synergistic catalytic benefits: cobalt cations contribute to high intrinsic ORR/OER activity through variable oxidation states and strong Co-O covalency, while vanadium cations enhance electronic conductivity and facilitate charge transfer through their multivalent nature ( $\text{V}^{3+}/\text{V}^{5+}$ ) [6]. The robust composition of  $\text{Co}_2\text{VO}_4$  ensures its stability even after being subjected to numerous electrical reactions. Cobalt vanadate ( $\text{Co}_2\text{VO}_4$ ) is a distinct compound formed from multiple metals, characterized by its unique crystal structure. The configuration of this structure determines how it responds to electrical forces, magnetic attractions, and chemical processes [4]. It operates like a semiconductor, which is useful in various light-driven and electronic technologies. Depending on temperature and structure, it may exhibit either ferrimagnetic or antiferromagnetic characteristics [7].

Cobalt vanadate is a mixed transition metal oxide that commonly crystallizes in a spinel-type structure ( $\text{AB}_2\text{O}_4$ ), where  $\text{Co}^{2+}$  occupies both tetrahedral (A) and octahedral (B) sites, and  $\text{V}^{5+}$  typically resides in the octahedral sites [4]. The crystal structure and cation distribution strongly influence its electrical, magnetic, and electrochemical properties.  $\text{Co}_2\text{VO}_4$  exhibits semiconducting behavior, often with a narrow bandgap, making it useful in photocatalytic and electronic applications. Due to the presence of magnetic  $\text{Co}^{2+}$  ions and potential  $\text{Co}^{3+}/\text{Co}^{2+}$  redox interactions,  $\text{Co}_2\text{VO}_4$  can exhibit ferrimagnetic or antiferromagnetic ordering, depending on temperature and structure [7]. The ability of cobalt and vanadium ions to undergo multiple oxidation states ( $\text{Co}^{2+}/\text{Co}^{3+}$  and  $\text{V}^{5+}/\text{V}^{4+}$ ) allows for high electrochemical activity [8].

Metal oxides are essential for the effective operation of metal-air batteries [9]. They enhance the air aspect of the battery by boosting two critical chemical reactions: the ORR that occurs while the battery is in use and the OER that takes place during the charging phase, especially for rechargeable batteries like zinc-air and lithium-air. Besides the ORR,  $\text{Co}_2\text{VO}_4$  also helps with the OER, which makes it a useful catalyst for rechargeable metal-air batteries [10]. The research employs Density Functional Theory (DFT) to investigate both the bulk and surface characteristics of  $\text{Co}_2\text{VO}_4$ , a material that has potential as a catalyst for zinc-air batteries. It is essential to develop a reliable and affordable catalyst to improve the functionality of zinc-air batteries.

## 2 Methodology

The calculations were done using a method called density functional theory (DFT) with a specific approach known as the generalized gradient approximation (GGA). We used the Perdew, Burke, and Ernzerhof (PBE) exchange-correlation functional to account for how particles interact with each other [11]. The number of plane waves was set based on a cut-off kinetic energy of 600 eV. To analyse the Brillouin zone of  $\text{Co}_2\text{VO}_4$  in both bulk form and on its surfaces, we employed the Monkhorst-Pack technique with a  $4 \times 4 \times 4$  grid for the bulk and a  $4 \times 4 \times 1$  grid for the surfaces. This approach was used to help integrate within the reciprocal space for all the lower Miller index surfaces. The METADISE code [12] was used to cut the surface of  $\text{Co}_2\text{VO}_4$ . We used Gaussian smearing with a width of 0.05 eV to make the geometry optimizations run more smoothly.

### 3 Results and discussions

#### 3.1 Structural properties

The  $\text{Co}_2\text{VO}_4$  structure, which is referred to as cobalt vanadate, is generally identified as spinel. Such a structure is frequently observed in various mixed metal oxides that adhere to the general formula  $\text{AB}_2\text{O}_4$ . The illustration in Figure 1 reveals the structure of the inverse spinel  $\text{Co}_2\text{VO}_4$ , indicating that cobalt ions are distributed across two types of sites, tetrahedral and octahedral, while vanadium ions are exclusively found in the octahedral sites. The cubic pattern, defined by the  $\text{Fd-}3\text{m}$  space group, organizes these shapes in a manner that is crucial to the material's special structural properties.

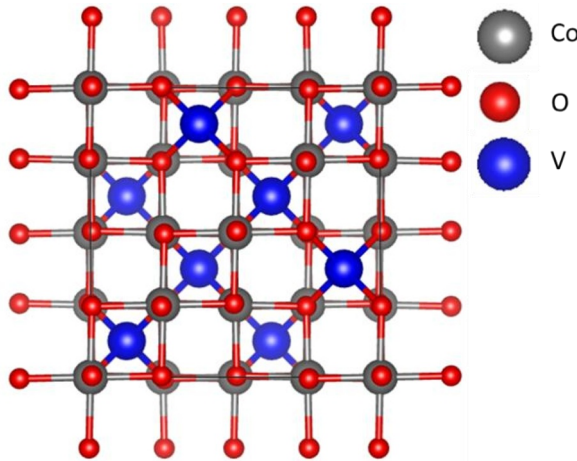


**Fig. 1.** The optimized bulk structure of  $\text{Co}_2\text{VO}_4$ .

The determined lattice parameters for  $\text{Co}_2\text{VO}_4$  are 3.22% different from the values found in literature. Several reasons may lead to this discrepancy. Discrepancies between fundamental calculations and experimental outcomes could be attributed to the constraints of DFT. This encompasses choosing the exchange-correlation functional, the pseudopotentials employed, and the method of sampling points within the system. For example, the GGA used in this work is known to slightly overestimate interatomic distances compared to experiment.

**Table 1.** The lattice parameters and bond distances are compared with the literature.

	Optimized $\text{Co}_2\text{VO}_4$	Literature
Lattice parameters	$a=b=c=8.116 \text{ \AA}$	$a=b=c=8.382 \text{ \AA}$ [4]
	$\alpha=\beta=\gamma=90.00^\circ$	$\alpha=\beta=\gamma=90.00^\circ$ [4]
Distance between atoms	Co-O = 1,989 $\text{ \AA}$ V-O = 1,827 $\text{ \AA}$	-

### 3.2 Electronic properties

Materials are divided into three key types: metals, semiconductors, and insulators. Different classifications arise from the size and existence of energy gaps located between the highest energy levels, known as the conduction band and valence band. The energy gap ( $E_g$ ) is the difference between the highest energy level of electrons that can form bonds ( $E_v$ ) and the lowest energy level where electrons can move freely ( $E_c$ ). The Fermi energy marks the limit between states that are occupied and those that remain unoccupied. There is a space between semiconductors and insulators, and this space is larger in insulators. The absence of gaps in the metal bands is due to the mixing of filled and unfilled orbitals. When there is a high density of states (DOS) at a given energy level, it suggests there are many potential vacancies for particles. On the flip side, a DOS of zero reflects that there are no positions currently available.

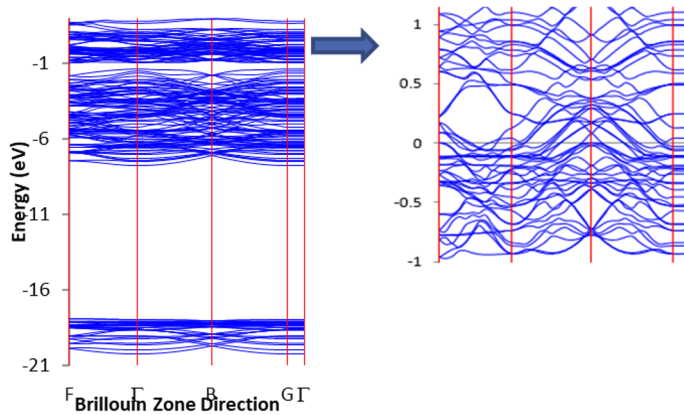


**Fig. 2.** The electronic band structure for  $\text{Co}_2\text{VO}_4$ .

#### 3.2.1 Electronic band structures

The calculated electronic band structures for  $\text{Co}_2\text{VO}_4$  affirm the nonappearance of a gap at the Fermi level. The absence of the gap resulted in overlap of orbitals at the Fermi level, thus, which makes the system a metal.

### 3.2.2 Density of states (DOS)

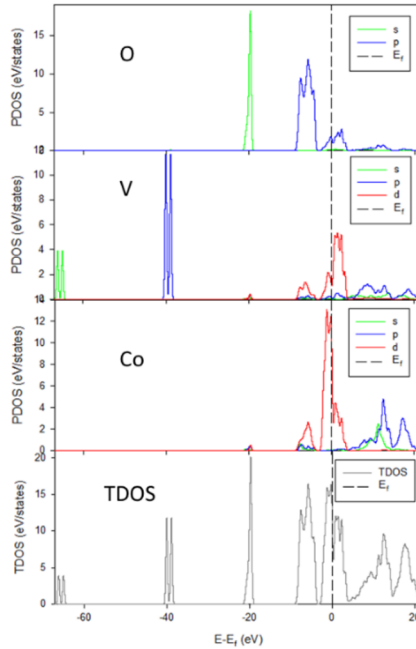


**Fig. 3.** The total density of states (TDOS) and the partial density of states (PDOS) corresponding to each atom in  $\text{Co}_2\text{VO}_4$  are examined.

The PDOS of oxygen atoms shows that s and p orbitals influence only the valence band, not the conduction band. Vanadium atoms have s, p, and d orbitals that shape valence and conduction bands. Cobalt atoms have s, p, and d orbitals in both bands, with the d orbital showing metallic behavior at the Fermi level for both the vanadium and cobalt atoms. Although there is a lower density of states around the Fermi energy, it still contains some occupancy. The formation of the pseudo gap is probably linked to the mixing of certain electron areas from V and Co, which may stem from electron interactions in transition metals. The DOS confirmed the metallic behaviour found from the electronic band structures, and the system remains stable at this level.

### 3.3 Surface properties

We cleaved the surfaces from the optimized bulk structure of  $\text{Co}_2\text{VO}_4$  using the lower Miller index surfaces (001), (011), and (111) systems. Upon cleaving the surfaces, the vacuum slab of  $17\text{\AA}$  was added to the system to avoid the interactions between periodic slabs. Calculations on the original slab are conducted to determine the unrelaxed surface ( $\gamma_u$ ) using a designated equation before relaxation:

$$\gamma_u = \frac{E_{slab,u} - E_{bulk}}{2A} \quad (1)$$

where  $E_{slab,u}$  is the total energy of the unrelaxed slab,  $E_{bulk}$  is the energy of the bulk having the same number of formula units as in the slab, and  $A$  is the surface area of the slab. Because this slab model accounts for both sides of symmetric slabs in energy calculations, it does not generate a separate relaxed surface. Two separate surface energy types are present:

$\gamma_r$  for the relaxed face and  $\gamma_u$  for the unrelaxed face. The energies are related through equation (2), which defines  $E_{slab,r}$  as the total energy of the slab following its relaxation.

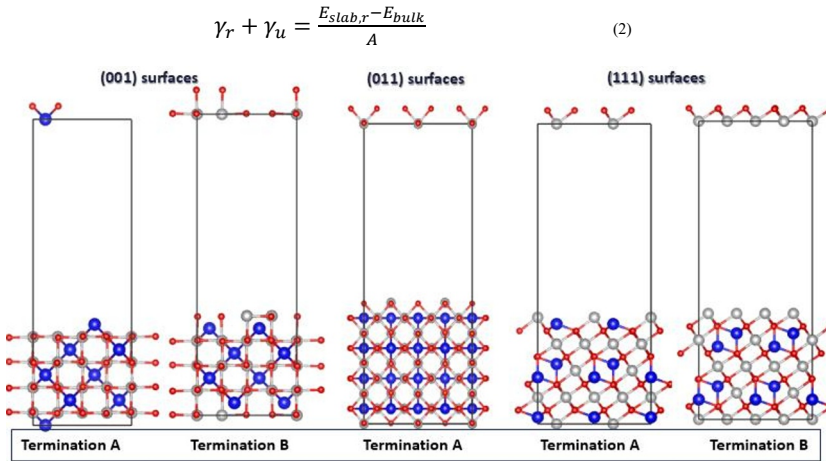


**Fig. 4.** Cleaved lower Miller index surfaces of  $\text{Co}_2\text{VO}_4$  with different terminations for the relaxed surfaces.

Table 2 below shows surface energies ( $\gamma$ ) for different terminations and orientations of  $\text{Co}_2\text{VO}_4$  surfaces, in both unrelaxed ( $\gamma_u$ ) and relaxed ( $\gamma_r$ ) states. The lowest surface energy indicates that the system is the most stable, while the highest surface energy suggests the least stable surface. Relaxation (atomic rearrangement at the surface) generally reduces the surface energy, thus increasing stability. The (001) Termination has the lowest relaxed surface energy ( $0.40 \text{ eV}/\text{\AA}^2$ ), indicating the highest thermodynamic stability among all considered surfaces. This suggests that this termination is most likely to appear in equilibrium crystal morphology. Relaxation significantly lowers surface energies across all terminations. Most pronounced change: (001) termination B drops from  $0.62 \rightarrow 0.47$  ( $\Delta = 0.15 \text{ eV}/\text{\AA}^2$ ). The least change: (111) termination A drops from  $0.56 \rightarrow 0.53$  ( $\Delta = 0.03 \text{ eV}/\text{\AA}^2$ ). The (001) surfaces are the most energetically favorable, especially termination A. The (011) surface is the least stable, even after relaxation. Relaxation plays a crucial role in enhancing surface stability, particularly for higher-energy terminations. The stability decreases in the following order: (001) A > (111) A > (011).

**Table 2.** Surface energies before  $\gamma_u$  and after relaxation  $\gamma_r$  for the  $\text{Co}_2\text{VO}_4$  system.

Surface	$\gamma_u$ ( $\text{eV}/\text{\AA}^2$ )	$\gamma_r$ ( $\text{eV}/\text{\AA}^2$ )
(001) Termination A	0,45	0,40
(001) Termination B	0,62	0,47
(011) Termination A	0,70	0,62
(111) Termination A	0,56	0,53
(111) Termination B	0,61	0,58

## 4 Conclusion

The density functional theory was successfully applied to determine the structural properties of the bulk, with lattice parameters and bond lengths in good agreement with those reported in the literature. The electronic band structures and density of states indicate that our bulk system exhibits metallic behavior due to the overlap of orbitals at the Fermi level. The contribution of each atom and its orbital contribution was strongly demonstrated; we noticed that the d orbital for vanadium and cobalt atoms contributes significantly at the Fermi level.

The metadise code was successfully utilized to model the (001), (011), and (111) surfaces, with the (001) surface identified as the most stable and (011) being the least stable. Because the (001) surface exhibits the highest stability, it is generally the side that appears in actual conditions. This makes it the most important surface to study for practical uses such as zinc adsorption, catalysis, or electronic devices. These findings provide insights into the properties of the  $\text{Co}_2\text{VO}_4$  bulk and surfaces.

The authors acknowledge the use of the National Integrated Cyber Infrastructure System (NICIS-CHPC) in Cape Town, South Africa, which is available via the Materials Modelling Centre (MMC) at the University of Limpopo.

This work is funded by the Materials Modelling Centre (MMC) and the National Research Foundation (NRF).

The data that support the findings of this study are available from the corresponding author upon reasonable request.

## References

- [1] X. Peng, T. Li, L. Zhong, J. Lu, Flexible metal–air batteries: An overview. *SmartMat.* **2**, 123-126 (2021). <https://doi.org/10.1002/smm2.1044>
- [2] T. Li, M. Huang, X. Bai, Y.X. Wang, Metal-air batteries: A review on current status and future applications. *Prog. Nat. Sci.-Mater. Int.* **33**, 151-171 (2023). <http://dx.doi.org/10.1016/j.pnsc.2023.05.007>
- [3] R.D. Al Bostami, A. Al Othoman, M. Tawalbeh, A.G. Olabi, Advancements in Zinc-Air Battery Technology and Water-Splitting. *WEF Nexus.* **17**, 100387 (2025). [10.1016/j.nexus.2025.100387](https://doi.org/10.1016/j.nexus.2025.100387)
- [4] C. Mu, J. Mao, J. Guo, Q. Guo, Z. Li, W. Qin, Z. Hu, K. Davey, T. Ling, S.Z. Qiao, Rational Design of Spinel Cobalt Vanadate Oxide  $\text{Co}_2\text{VO}_4$  for Superior Electrocatalysis. *Adv. Mater.* **32**, 1907168 (2020). <https://doi.org/10.1002/adma.201907168>
- [5] D. Mladenovic, A. Mladenovic, D.M. Santos, A.B. Yurtcan, S. Miljanic, S. Mentus, B. Sljukic, Transition metal oxides for bifunctional ORR/OER electrocatalysis in unitized regenerative fuel cells. *J. Electroanal. Chem.* **946**, 117709 (2023). <https://doi.org/10.1016/j.jelechem.2023.117709>
- [6] W. Liu, M. Kamiko, I. Yamada, S. Yagi, Effects of cation vacancies at tetrahedral sites in cobalt spinel oxides on oxygen evolution catalysis. *Mater. Adv.* **3**, 7513-7519 (2022). <https://doi.org/10.1039/D2MA00729K>
- [7] N.I. Abu-Elsaad, A.S. Nawara, Effect of Cu substitution on magnetic and photocatalytic properties of Mn– $\text{ZnFe}_2\text{O}_4$  nanoparticles. *J. Mater. Sci.* **59**, 4167-4185 (2024). <https://doi.org/10.1007/s10853-024-09486-8>
- [8] A.A. Jadhavar, N.T. Shelke, M.A. Yewale, R.A. Kadam, S.L. Kadam, D.K. Shin, Hydrothermal synthesis of cobalt vanadium oxide ( $\text{Co}_3\text{V}_2\text{O}_8$ ) hexagonal disc for

- high-performance supercapacitors. SURF INTERFACES. **43**, 103519 (2023).  
<https://doi.org/10.1016/j.surfin.2023.103519>
- [9] A.E. Hughes, N. Haque, S.A. Northey, S. Giddey, Platinum group metals: A review of resources, production and usage with a focus on catalysts. Resour. **10**, 93 (2021).  
<https://doi.org/10.3390/resources10090093>
- [10] J. Liu, Y. Ji, J. Nai, X. Niu, Y. Luo, L. Guo, S. Yang, Ultrathin amorphous cobalt–vanadium hydr (oxy) oxide catalysts for the oxygen evolution reaction. Energy Environ. Sci. **11**, 1736-1741 (2018). <https://doi.org/10.1039/C8EE00611C>
- [11] S.C. Abrahams and J.L. Bernstein, Rutile: normal probability plot analysis and accurate measurement of crystal structure. Chem. Phys. **55**, 3206-3211 (1971).  
<https://doi.org/10.1063/1.1676569>
- [12] G.W. Watson, E.T. Kesley, N.H. de Leeuw, D.J. Harris, S.C. Parker, Atomistic simulation of dislocations, surfaces, and interfaces in MgO. J. Chem. Soc. **92**, 433-438 (1996). <https://doi.org/10.1039/FT9969200433>